Shap. Mem. Superelasticity (2016) 2:80–85
DOI 10.1007/s40830-016-0055-2

Composition–Structure–Property Relations in $Au_{35–68}Cu_{49–15}Al_{16–17}$ Shape Memory Thin Films

Pio John S. Buenconsejo[1,2] · Janine Pfetzing-Micklich[1] · Michael Paulus[3] · Christian Sternemann[3] · Alfred Ludwig[1]

Published online: 22 February 2016

Abstract The phase transformation behaviour, structure and mechanical properties of $Au_{35–68}Cu_{49–15}Al_{16–17}$ thin film shape memory alloys (SMA) have been investigated, with emphasis on the effects of Au content. The results revealed the underlying composition–structure–property relations. The thermal transformation hysteresis (ΔT) is wide ($\sim$55 K) for thin films with Au <50 at.%, while it is narrow ($\sim$15 K) for thin films with Au >50 at.%. This behaviour is correlated with the change in lattice constant of β-(Au–Cu–Al) ($\mathbf{a_\beta}$), suggesting a structural origin on the ΔT behaviour. The mechanical properties, such as hardness and elastic modulus, varied in the range of 2–4 and 70–120 GPa, respectively. The optimum Au composition range for tuning the functional property is between 43 and 55 at.% Au, where the least amount of non-transforming phases form and ΔT can be tailored between 55 K (43 at.% Au) and 17 K (55 at.% Au). This is important for the development and practical application of Au–Cu–Al based thin film SMA.

✉ Pio John S. Buenconsejo
pbuenconsejo@ntu.edu.sg

✉ Alfred Ludwig
alfred.ludwig@rub.de

[1] Institute for Materials, Ruhr-Universität Bochum, 44801 Bochum, Germany

[2] Facility for Analysis Characterisation Testing and Simulation (FACTS), School of Materials Science and Engineering, Nanyang Technological University, Singapore 639798, Singapore

[3] Fakultät Physik/DELTA, Technische Universität Dortmund, 44221 Dortmund, Germany

Keywords Au–Cu–Al · Shape memory alloys · Thin films · Phase transformations

Introduction

A well-known composition in the Au–Cu–Al system is the $Au_7Cu_5Al_4$ 'Spangold' shape memory alloy (SMA) [1–4]. This is the β-phase in the Au–Cu–Al system [3] and it undergoes reversible structural transformation to a martensite phase [4, 5]. The structure of the parent β-(Au–Cu–Al) phase is bcc [3], while the structure of the martensite phase has been recently clarified as being either orthorhombic or monoclinic, depending on the composition and temperature of the alloy [5]. These SMAs are promising for jewellery and biomedical applications, due to their inherent properties, such as biocompatibility, aesthetic value and chemical inertness. However, most investigations were performed on bulk alloys so far [1–9] and very few studies have been devoted to thin films [10, 11].

Recently, a comprehensive study of the Au–Cu–Al system by thin film combinatorial synthesis and high-throughput experimentation revealed a wide range of new potential thin film SMA compositions [11]. It was found that the phase transformation properties of β-(Au–Cu–Al) can be tuned over a large composition space. The transformation temperatures can be adjusted from below room temperature to above 100 °C, while the transformation hysteresis varies from 15 to 65 K. The possibility to tune functional properties over a wide composition range is beneficial for potential applications. For example, SMAs with a wide hysteresis are good for superelasticity, while a narrow hysteresis is beneficial for fast actuation. The results of the former study already extended potential

applications of Au–Cu–Al-based SMAs. However, in order to further optimize the properties, it is important to understand the influence of composition on the structure and property of these alloys.

The β-(Au–Cu–Al) phase is a β electron alloy [3–5], and its stability is proportional to the electron per atom ratio (*e*/*a*). The *e*/*a* ratio of an alloy is determined by its constituent elements and composition. As Au and Cu are monovalent, while Al is trivalent, the *e*/*a* ratio of β-(Au–Cu–Al) phase is only dependent on the Al content. A high *e*/*a* ratio stabilizes the β-(Au–Cu–Al) phase, which means that the martensitic transition is shifted towards lower temperatures. This trend was confirmed in the thin film combinatorial investigation of the Au–Cu–Al system [11]. Furthermore, the martensitic transformation start (M_s) and reverse transformation finish (A_f) temperatures decrease with increasing Al content. The transformation hysteresis ($\Delta T = A_f - M_s$) follows a different trend. The ΔT for thin films with Al <15 at.% did not show any significant composition dependence; however for thin films with Al >15 at.%, ΔT varies with the Au content.

The goal of this study is to investigate the effects of Au content on the structure–property relations of $Au_{35–68}Cu_{49–15}Al_{16–17}$ thin film SMAs. In order to exclude the influence of the Al content on the phase transformation temperatures, samples with constant Al content (16–17 at.%) were selected from the Au–Cu–Al materials library.

Experimental Procedure

The thin films investigated in this study were selected compositions from a Au–Cu–Al thin film materials library. The materials library was made using a thin film combinatorial sputter deposition system (DCA Finland). Each element was deposited as a thickness wedge across the substrate (4-in. (100)-Si with 1.5 µm thick SiO_2 diffusion barrier) and the wedge directions were oriented 120° away from each other. The whole process was repeated until a $(Au/Cu/Al)_{30}$ multilayer thin film precursor continuous composition spread was made across the surface of the substrate. Measurement regions corresponding to specific compositions in the materials library were defined by applying a measurement grid of 4.5 mm by 4.5 mm size. The multilayer precursor materials library was annealed at 500 °C for 1 h (in UHV) to allow mixing, interdiffusion and phase formation. Composition mapping was made by using a scanning electron microscope (JEOL JSM 5800LV) equipped with an energy dispersive X-ray detector (Oxford INCA 250 system). The detailed results on the characterisation and screening of properties were reported in [11].

For this study, the focus is to elucidate the effects of Au content on the phase transformation behaviour and mechanical properties, so the compositions of $Au_{35–68}Cu_{49–15}Al_{16–17}$ were selected. The nearly constant Al content eliminates the effects of the *e*/*a* ratio on the phase transformation behaviour. The effects are therefore solely due to varying Au (or Cu) content. From here onwards only the Au content of the alloys will be indicated.

The phase transformation behaviour (transformation temperatures, hysteresis widths) was characterized by measuring the electrical resistance (4-point probe) during thermal cycles in the temperature range between −20 and 250 °C [12]. The collected data are presented as $R(T)$ curves on cooling and heating.

To carry out phase analysis with high spatial resolution, the selected composition range was investigated by X-ray diffraction analysis performed at beamline BL9 of DELTA synchrotron radiation source [13] using a MAR345 image plate detector with a beam spot of 0.2 × 1 mm^2 ($v \times h$) and a wavelength of 0.0459 nm. The X-ray diffraction profile of the selected composition range was collected at an incident angle of 5° with respect to the sample surface in order to suppress the contribution of the substrate. Polycrystalline Si was used for calibrating the geometry of the diffraction set-up. The fit2D software [14] was applied for converting the data after collection. The X-ray diffraction data were used for phase identification and to calculate the lattice constant $\mathbf{a_\beta}$ of the β-(Au–Cu–Al) phase.

Film texture was evaluated using a Bruker D8 Discover with an Eulerian stage. The pole figures (PF) of β-(Au–Cu–Al) phase were collected at the following *hkl* planes: (200), (220) and (222). This measurement was carried out on selected samples after they were separated from the materials library by dicing.

Young's modulus and hardness of the selected compositions were evaluated using high-throughput nanoindentation [15, 16]. The nanoindenter (XP, MTS) with a Berkovich tip was used to collect data using continuous stiffness measurements (CSM) up to a maximum indentation displacement of 50 nm. The indentation depth is less than 10 % of the film thickness such that substrate effects are considered negligible. For each composition, 5 indents were made with at least 50 µm distance from each indent.

Results

X-ray diffraction profiles of the thin films are shown in Fig. 1. The profiles revealed the phases that formed by annealing at 500 °C for 1 h. The phases were identified using the Pearson database [17], while the β-(Au–Cu–Al)

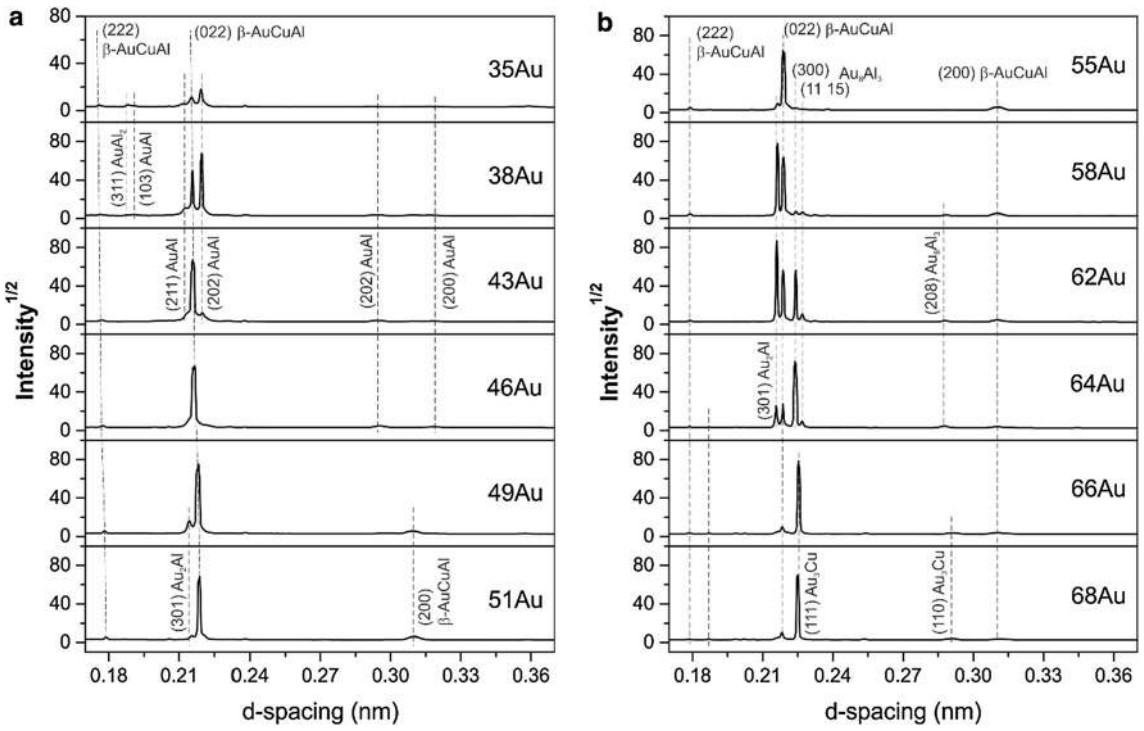

Fig. 1 X-ray diffraction profiles of $Au_{35–68}Cu_{49–15}Al_{16–17}$ thin films taken at room temperature: **a** for samples with Au contents between 35 and 51 at.%, **b** for samples with Au contents between 55 and 68 at.%. The Au content is indicated for each profile. The *x*-axis is given in *d*-spacing (nm) values, while the intensity is in square root in order to make the small diffraction peaks visible with respect to the large diffraction peaks

phase was indexed based on its reported structure [3]. The phase transforming phase (β-(Au–Cu–Al)) formed together with non-transforming phases (Au_3Cu, Au_2Al, Au_8Cu_3, AuAl, and $AuAl_2$). The β-(Au–Cu–Al) phase is present in all samples. The type of non-transforming phases changed with Au content. Based on the peak intensity, β-(Au–Cu–Al) is mostly predominant between 43 and 55 at.% Au. Outside this range the non-transforming phases are predominant. From the Au-rich side, the Au_3Cu phase was prominent for <64 at.% Au, and between 55 and 64 at.% the phase constitution became a mixture of Au_2Al, Au_8Cu_3 and β-(Au–Cu–Al) phases. For the Au-poor side (<43 at.%) the AuAl and $AuAl_2$ phases were predominant.

To determine the preferred crystallographic orientation of the β-(Au–Cu–Al) phase in the thin films, PF of various *hkl* planes ((022), (200) and (222)) was measured. A typical set of PFs, measured from the 51Au thin film, is shown in Fig. 2a. It can be deduced from the PFs that the thin film has a very strong fibre texture with a [022] out-of-plane fibre axis direction. This type of film texture was confirmed for all samples regardless of Au content, as shown by the (022) PFs of the representative samples in Fig. 2b. The maximum intensity (*I*-max) varied slightly (slightly dropping at the lowest and highest Au contents). No other texture components can be confirmed from the PFs.

The phase transformation behaviour of the investigated thin films having different Au contents is shown as $R(T)$ curves in Fig. 3a. Phase transformation temperatures (M_s and A_f) are indicated by arrows. There is a clear dependence of transformation behaviour with respect to Au composition, where M_s varied only slightly but A_f significantly changed. As a consequence, the thin films with Au <51 at.% show a wide transformation hysteresis ΔT compared to thin films with Au >51 at.%. For example ΔT of 35Au is about 65 K, while it is about 16 K for 62Au.

The results of nanoindentation experiments of representative samples are shown as load–displacement curves in Fig. 3b. The averaged hardness (H) and elastic modulus (E) of 51Au are 2.5 and 75 GPa, respectively. The H and E values are higher for compositions deviating from 51Au. Additionally, the standard deviations are larger for compositions deviating from 51Au. These trends are explained below (Fig. 4) in conjunction with the structure and composition of the films.

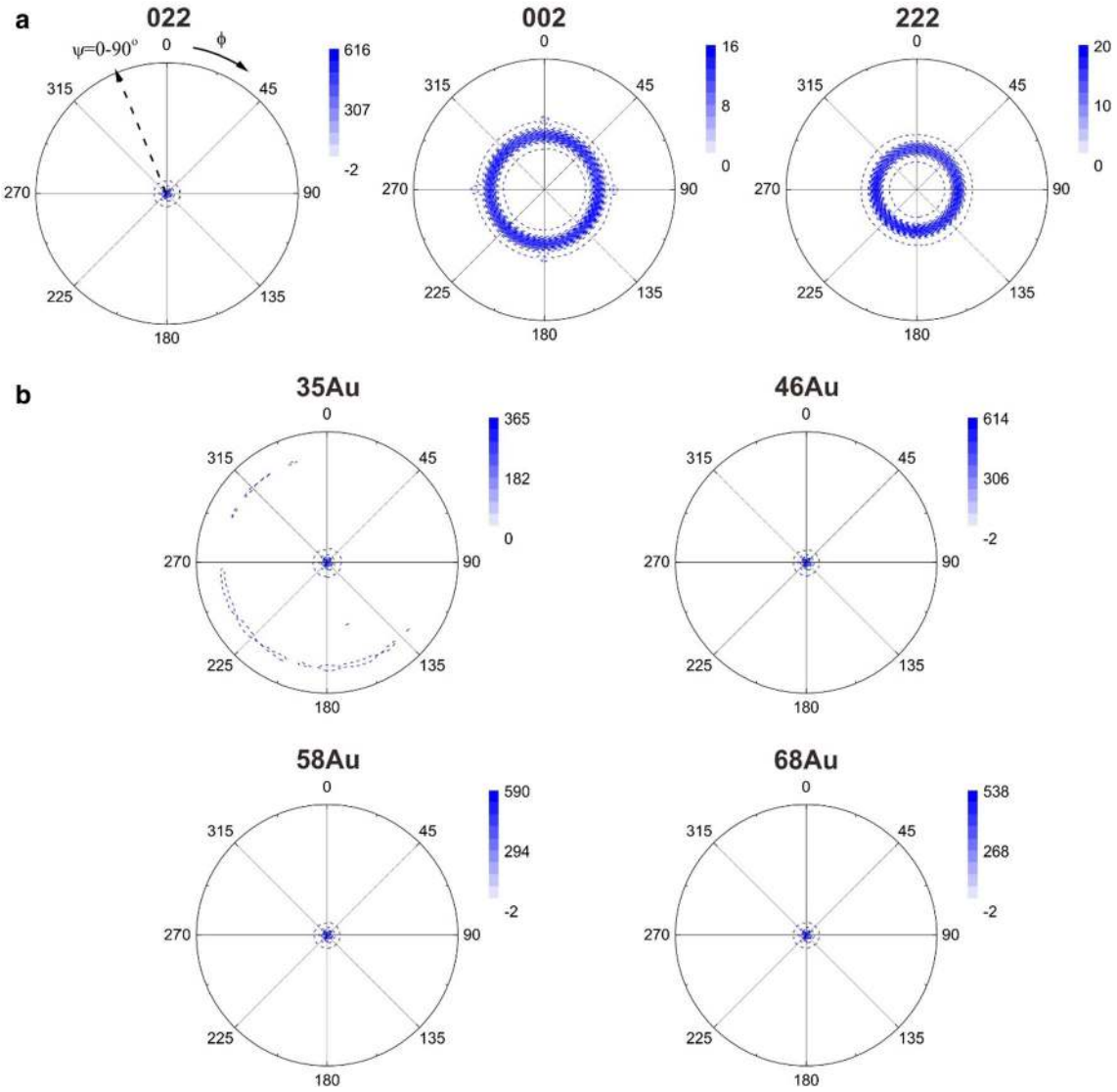

Fig. 2 **a** Pole figures (PF) measured on 51Au SMA thin film at different *hkl* planes (022), (002), (222)) of β-(Au-Cu-Al) phase. **b** Representative PF of (022) planes for alloys with Au contents from 35 to 68 at.%

Discussion

All experimental results are combined into a composition–structure–property relations diagram, which is presented in Fig. 4. It shows a comparison of phase constitution (Fig. 4a), lattice constants (Fig. 4b), phase transformation temperatures (Fig. 4c) and mechanical properties (Fig. 4d) with respect to Au content.

The phase and texture of the films determined from the diffraction data and PFs are summarized in Fig. 4a. Au-poor (<50 at.%) compositions form $AuAl_2$ and AuAl phases, while Au-rich (>50 at.%) compositions form Au_2Al, Au_8Al_3 and Au_3Cu. Therefore, the formation of non-transforming phases is dependent on the ratio of Au with respect to Cu or Al. The β-(Au–Cu–Al) phase formed in all investigated compositions, but its amount (estimated based on peak intensity) decreases with increasing Au or Cu content in the alloy. Furthermore, the [011] fibre texture of the β-(Au–Cu–Al) phase remained the same regardless of Au content. This type of texture is typical for thin films with a bcc structure.

Figure 4b shows the plot of lattice constants values ($\mathbf{a_\beta}$) with respect to Au. The values of $\mathbf{a_\beta}$ range from 0.610 to 0.620 nm, comparable with values reported in the literature [3]. For thin films with Au content between 43 and 51 at.%, $\mathbf{a_\beta}$ increases with increasing Au. For thin films with Au >51 at.% and Au <43 at.%, $\mathbf{a_\beta}$ approached constant values. The change in $\mathbf{a_\beta}$ is related to the solubility of elements in the crystal structure of β-(Au–Cu–Al) phase. This effect is due to the differences of the metallic radius (Au 144 pm, Cu 128 pm, Al 143 pm) [18]. The amount of Al is constant

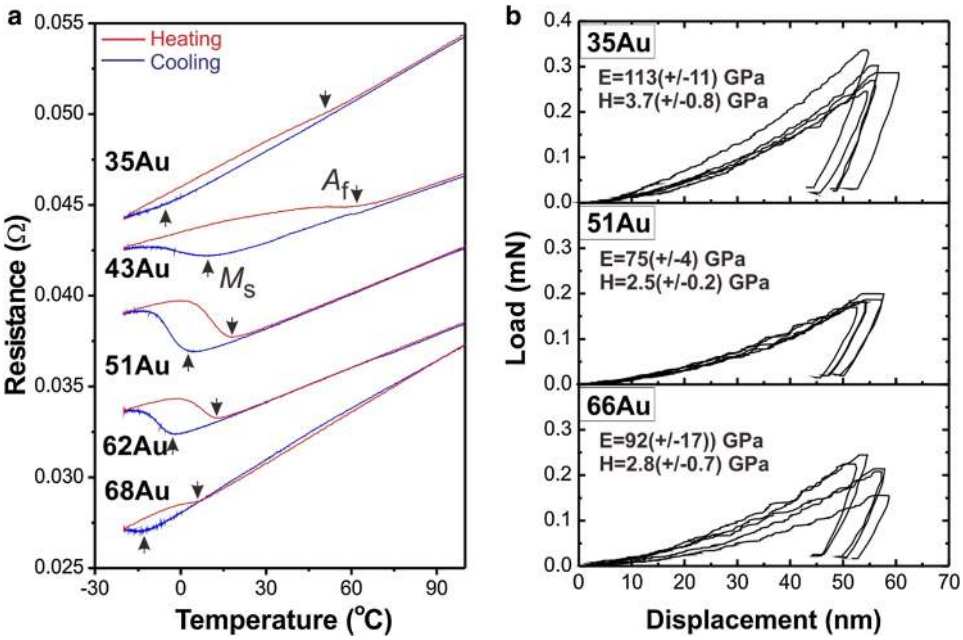

Fig. 3 **a** Selected resistance–temperature curves of $Au_{35–68}Cu_{49–15}Al_{16–17}$ thin films, where M_s and A_f are the martensite transformation start and reverse transformation finish temperatures, respectively. **b** Exemplary load–displacement *curves* of Au–Cu–Al thin films, measured using nanoindentation method (5 measurements for each composition)

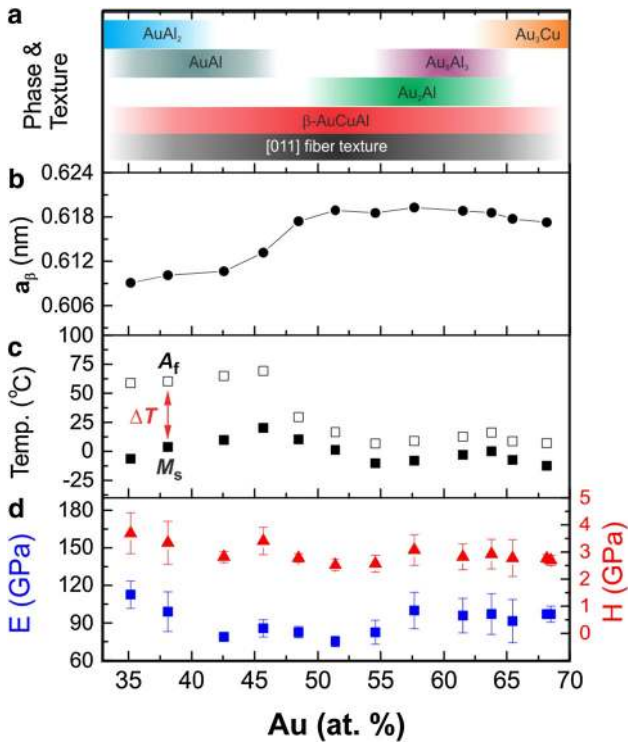

Fig. 4 A summary of structure–property relations of $Au_{35–68}Cu_{49–15}Al_{16–17}$ SMA thin films. **a** The existence range of the observed phases is indicated by the coloured boxes, the [011] fibre texture is observed for all compositions; **b** lattice constant values derived from X-ray diffraction data; **c** transformation temperatures and hysteresis widths derived from $R(T)$ measurements, and **d** mechanical properties (Young's modulus E (*squares*), hardness H (*triangles*)) obtained by nanoindentation

for all samples; therefore, the change in $\mathbf{a_\beta}$ is only influenced by the difference in Au (or Cu) content. The high Cu content alloys have smaller $\mathbf{a_\beta}$, while the high Au content alloys have larger $\mathbf{a_\beta}$ due to the difference of their metallic radius. In the range between 43 and 51 at.% Au, the pronounced change in $\mathbf{a_\beta}$ could be attributed to the substitution effects of Cu and Au. This is also the region with the least amount of non-transforming phases. The value of $\mathbf{a_\beta}$ for thin films with Au >51 at.% and Au <43 at.% approached a nearly constant value, indicating the maximum solubility of Au and Cu, respectively, in the β-(Au–Cu–Al) phase. In order to balance the stoichiometry the excess elements form the non-transforming phases.

The dependence of the phase transformation temperatures on composition (Fig. 4c) is as follows: M_s is almost constant but A_f varies with Au content. The almost constant M_s is assigned to the constant Al content of the alloys. As a result the observed ΔT varies with Au content. Specifically below 47 at.% Au ΔT is more than 50 K, while above 47 at.% Au ΔT is less than 20 K. Interestingly the observed trend for ΔT follows the trend of $\mathbf{a_\beta}$, suggesting a structural origin of the hysteresis behaviour. In this case a wide ΔT is confirmed for smaller $\mathbf{a_\beta}$, while a narrow ΔT is confirmed for larger $\mathbf{a_\beta}$. In the general non-linear theory of martensitic transformation, the lattice constants of the parent and martensite phases play an important role in controlling ΔT [19]. The same mechanism is assumed to be behind the ΔT behaviour observed in this study. However, this cannot be confirmed because the lattice constant of the martensite phase was not measured. This will be a subject of future investigations in this new SMA system.

The mechanical properties are presented in Fig. 4d. The E varied between 75 and 115 GPa, while hardness H varied between 2.5 and 4 GPa. The lowest E was found in the range of 43Au to 55Au, corresponding to the composition range with the smallest amount of non-transforming phases. Thus, the E of the β-(Au–Cu–Al) phase can be estimated to be in the range of 75–85 GPa. Outside the 43 at.% > Au > 55 at.% composition range, the E values and their standard deviations are higher due to the presence of various phases in the respective measurement areas, having different mechanical properties. Using the rule of mixture, the resulting H and E values will be the average of the various phases present. Similarly for the H values, a high standard deviation is typically observed for compositions with mixed phases. This behaviour is consistent with previous nanonindentation study of NiTi bulk alloy, where it was found that large amount of phase transformation tends to show lower E and H values during nanoindentation [20].

Therefore, the optimum Au composition range is between 43 and 55 at.%. This range has the smallest amount of non-transforming phases, so it contains the maximum volume fraction of transforming phase in the material. Additionally ΔT can be tuned between 15 and 55 K.

Conclusion

The effects of Au content on the structure and materials properties of $Au_{35–68}Cu_{49–15}Al_{16–17}$ SMA thin films have been clarified in this study. The results are summarized into a composition–structure–property diagram revealing important correlations. The optimum Au content is between 43 and 55 at.%, since it contains minimal amount of non-transforming phases. It is also the composition range where ΔT is tunable from 15 to 55 K. A good correlation between ΔT and $\mathbf{a_\beta}$ was confirmed suggesting a structural origin of the hysteresis behaviour in this SMA system. Lastly the elastic modulus of the β-AuCuAl phase is in the range of 75–85 GPa and hardness in the range of 2.5–3.4 GPa.

Acknowledgments The authors would like to express their gratitude for support from the German Research Foundation (DFG) within the FOR 1766 (High temperature shape memory alloys) research funding. We also acknowledge the synchrotron beam time granted to us by the DELTA synchrotron radiation source in Dortmund, Germany. We also acknowledge the use of Bruker D8 Discover XRD facility in FACTS, NTU, Singapore.

References

1. Cortie M, Wolff I, Levey F, Taylor S, Watt R, Pretorius R, Biggs T, Hurly J (1994) Spangold, a jewellery alloy with an innovative surface finish. Gold Technol 14:30–36
2. Levey FC, Cortie MB, Cornish LA (2000) Displacive transformations in Au-18 wt pct Cu-6 wt pct Al. Metall Mater Trans 31A:1917–1923
3. Cortie MB, Levey FC (2000) Structure and ordering of the 18-carat Al–Au–Cu β-phase. Intermetallics 8:793–804
4. Levey FC, Cortie MB (2001) Body-centred tetragonal martensite formed from Au 7 Cu 5 Al 4 β phase. Mater Sci Eng A 303:1–10
5. Elcombe MM, Kealley CS, Bhatia VK, Thorogood GJ, Carter DJ, Avdeev M, Cortie MB (2014) Determination of martensite structures of the Au 7 Cu 5 Al 4 and Au 7 Cu 5.7 Al 3.3 shape-memory alloys. Acta Mater 79:234–240
6. Fumagalli L, Besseghini S, Passaretti F, Airoldi G (2007) Thermoelastic martensitic transformation in Au–Cu–Al alloys doped with Co or Ir. J Alloy Compd 433:332–337
7. Gu Y, Jin M, Jin X (2009) A2→ B2→ L2 1 ordering transitions in Au–Cu–Al alloys. Intermetallics 17:704–707
8. Jin M, Liu J, Jin X (2010) Ordering transitions in quenched Au 7 Cu 5 Al 4 alloy and effect of order on martensitic transformation. Intermetallics 18:846–850
9. Fiore G, Battezzati L (2011) An entropy driven phase transformation in a Au 43.3 Cu 31.8 Al 24.9 shape-memory alloy. Intermetallics 19:1978–1982
10. Bhatia V, Thorogood G, Dowd A, Cortie MB (2011) Thin films of AuCuAl shape memory alloy for use in plasmonic nano-actuators. MRS Proc 1295:33–38
11. Buenconsejo PJS, Ludwig A (2015) New Au–Cu–Al thin film shape memory alloys with tunable functional properties and high thermal stability. Acta Mater 85:378–386
12. Thienhaus S, Hamann S, Ludwig A (2011) Modular high-throughput test stand for versatile screening of thin-film materials libraries. Sci Technol Adv Mater 12:054206
13. Krywka C, Sternemann C, Paulus M, Javid N, Winter R, Al-Sawalmih A, Yi S, Raabe D, Tolan M (2007) The small-angle and wide-angle X-ray scattering set-up at beamline BL9 of DELTA. J Synchrotron Radiat 14:244
14. Hammersley AP (1998) FIT2D V9.129 Reference Manual V3.1, ESRF Internal Report, (ESRF98HA01T)
15. Zarnetta R, Kneip S, Somsen C, Ludwig A (2011) High-throughput characterization of mechanical properties of Ti–Ni–Cu shape memory thin films at elevated temperature. Mater Sci Eng A 528:6552–6557
16. Thienhaus S, Naujoks D, Pfetzing-Micklich J, Koenig D, Ludwig A (2014) Rapid identification of areas of interest in thin film materials libraries by combining electrical, optical, X-ray diffraction, and mechanical high-throughput measurements: a case study for the system Ni–Al. ACS Comb Sci 16:686–694
17. Villars P, Cenzual K (2012/13) Pearson's crystal data: crystal structure database for inorganic compounds (on DVD). ASM International®, Materials Park
18. Pearson WB (1972) Crystal chemistry and physics of metals and alloys. Wiley, Chichester
19. Zarnetta R, Takahashi R, Srivastava V, Young ML, Savan A, Furuya Y, Thienhaus S, Maass B, Rahim M, Frenzel J, Brunken H, Chu YS, James RD, Takeuchi I, Eggeler G, Ludwig A (2010) Identification of quaternary shape memory alloys with near-zero thermal hysteresis and unprecedented functional stability. Adv Funct Mater 20:1917–1923
20. Pfetzing-Micklich J, Somsen C, Dlouhy A, Begau C, Hartmaier A, Wagner MF-X, Eggeler G (2013) On the crystallographic anisotropy of nanoindentation in pseudoelastic NiTi. Acta Mater 61:602–616